Article

Not peer-reviewed version

Uplift and Denudation History of the Jianfeng Pluton on Hainan Island, China

Di Lin , Guicheng Xue , Yong Zheng * , Gucheng Zhang * , Zailong Hu , Changxin Wei , Zhizhuang Zhang , Qinmin Yuan

Posted Date: 21 February 2025

doi: 10.20944/preprints202502.1758.v1

Keywords: Hainan Island; Yinggehai Basin; uplift and denudation; Cooling history; dynamic mechanism

Article

Uplift and Denudation History of the Jianfeng Pluton on Hainan Island, China

Di Lin [1,2], Guicheng Xue [1,2], Yong Zheng [3,4,5,*], Gucheng Zhang [1,2,6,*], Zailong Hu [1,2], Changxin Wei [1,2], Zhizhuang Zhang [2] and Qinmin Yuan [2]

[1] Hainan Key Laboratory of Marine Geological Resources and Environment, Haikou, Hainan 570206 , China; lindi1104125@163.com; 13876097165@163.com; lindi2004@163.com; chx_wei@126.com

[2] Hainan Provincial Institute of Geological Survey, Hainan, Haikou, Hainan 570206, China; todobig@sohu.com; lindi@163.com

[3] SinoProbe Laboratory, Key Laboratory of Continental Dynamics of Ministry of Natural Resources, Institute of Geology, Chinese Academy of Geological Sciences, Beijing 100037, China ;

[4] Jiangsu Donghai Continental Deep Hole Crustal Activity National Observation and Research Station, Lianyungang, Jiangshu 222300, China ;

[5] Southern Marine Science and Engineering Guangdong Laboratory (Guangzhou), Guangzhou, Guangdong 511458, China;

[6] School of Earth Sciences, China University of Geosciences, Wuhan 430074, China;

* Correspondence: zygeology@126.com (Y.Z.); zhanggucheng2000@163.com (G.Z.)

Abstract: Hainan Island is the only large island located on the northern margin of the South China Sea and is surrounded by Cenozoic graben basins, including the Qiongdongnan, Yinggehai, and Beibuwan basins. The uplift and denudation history of the Jianfeng pluton on southwestern Hainan Island is significant for understanding the formation of the regional geomorphology and adjacent basin evolution. This paper presents apatite and zircon fission-track (FT) analyses conducted on the Jianfeng pluton. The zircon FT (ZFT) ages of the pluton range from 63 ± 4 to 117 ± 8 Ma, and the apatite FT (AFT) ages from 19.4 ± 1.8 to 43.9 ± 4.4 Ma. The average confined track lengths in apatite are relatively short (11.9–12.8 μm). An age–elevation plot indicates that two rapid cooling events occurred during 73–63 and 44–40 Ma. Thermal modeling revealed four stages of 73-63 Ma, 44-40 Ma, 40-11 Ma and 11-0 Ma. From the Late Cretaceous to middle Eocene (73–40 Ma), the Jianfeng area underwent episodic rapid uplift and denudation. At the end of the Late Cretaceous (73–63 Ma), the area was affected by mid-ocean ridge spreading in the Proto-South China Sea. During the middle Eocene (44–40 Ma), the Yinggehai Basin underwent abrupt expansion and subsidence, which increased the elevation difference between the Jianfeng area and the Yinggehai Basin. From the middle Eocene to middle Miocene (40–11 Ma), the Jianfeng area underwent slow denudation and the Yinggehai Basin was rapidly infilled, which eliminated the original elevation difference between the two areas. From the middle Miocene to present (11–0 Ma), the Jianfeng area has undergone reactivated rapid uplift and denudation, driven by the remote effects of India–Eurasia collision.

Keywords: Hainan Island; Yinggehai Basin; uplift and denudation; Cooling history; dynamic mechanism

1. Introduction

Hainan Island is located at the intersection of the Eurasian, Indian, and Pacific plates [1,2]. It is the only large island above sea-level on the northern margin of the South China Sea. The island is surrounded by the Qiongdongnan, Yinggehai, and Beibuwan basins, which form the framework of the basin–mountain structure of the region [3,4]. The proximal coarse-grained clastic sediments resulting from the uplift and denudation of Hainan Island now comprise important reservoirs in the surrounding Cenozoic oil and gas basins [5-7]. Consequently, the uplift and denudation history of

 doi:10.20944/preprints202502.1758.v1

Hainan Island is essential for understanding the sedimentary dynamics of the surrounding basins [8,9].

The peaked Jianfeng mountain is located in southwestern Hainan Island, near the Yinggehai Basin. The main peak, with an altitude of 1412 m, contrasts sharply with the Yinggehai Basin and surrounding hilly terrain to the west. It is the most significant geological tourism area in the National Park of Hainantropical Rainforest and is of considerable scientific and tourist interest. It is the main place to understand the sedimentary history of adjacent basins and the Cenozoic tectonic evolution of the region. The Jianfeng pluton is the primary geological feature in the Jianfeng scenic area within the national park. Due to the proximity of the Baolun Au deposit to the margin of the Jianfeng pluton, previous studies have investigated the petrogenesis and tectonic setting of the pluton, and its relationship to Au mineralization [10-12]. However, there have been no quantitative studies of the uplift and denudation of the pluton, which were important in the formation of the granite landforms and sedimentary history of the adjacent basins. This has resulted in an incomplete understanding of the geoscientific significance of the national park.

Fission-track (FT) dating can be used to reconstruct the uplift and denudation history of the shallow crust and constrain the effects of regional tectonic changes, due to its relatively low annealing temperature and track length variations produced when a mineral resides within the partial annealing zone (PAZ) [13-16]. This paper presents new apatite (AFT) and zircon fission-track (ZFT) analyses of the Jianfeng pluton. We constrained the uplift age, cooling rate, and rate and amount of denudation of the Jianfeng pluton since the late Mesozoic. In addition, we determined the uplift and denudation mechanisms of Hainan Island since the late Mesozoic. These results enhance our understanding of the geoscientific significance of the national park and can guide exploration for oil and gas in the basins around Hainan Island.

2. Geological Setting

Hainan Island is a long-exposed, continental margin island located on the northern margin of the South China Sea, separated from mainland South China by the Qiongzhou Strait. Its topography is characterized by high elevations in the center of the island [17]. Hainan Island is located in the footwall of the main boundary fault of the surrounding Cenozoic graben basins, including the Qiongdongnan, Yinggehai, and Beibuwan basins (Figure 1a). The island is located near the intersection of the Eurasian, Indian, and Pacific plates, and has been affected by the Tethyan and Pacific tectonic domains [1,4,18,19]. Its structural features are relatively complex, with faults being the dominant structures, which were formed by collision and compression during the Hercynian–Indosinian orogenies, extensional faulting during the Yanshanian Orogeny, and further rifting during the Himalayan Orogeny [20,21]. Throughout the Cenozoic, the structure of Hainan Island has remained relatively stable. The pre-Cenozoic faults along its margins have been continuously active, particularly the E–W-trending Wangwu–Wenjiao, NE–SW-trending Binhai, and NW–SE-trending Puqian faults (Figure 1b). These faults have controlled the Cenozoic sedimentation and magmatism on the island [3]. The strata on the island are relatively complex, and include Mesoproterozoic to Quaternary rocks, but no Devonian or Jurassic strata. The Mesoproterozoic Baoban Group comprises gneisses and migmatites that have undergone amphibolite-facies metamorphism. The upper Proterozoic Shilu Group consists of schists that have undergone greenschist-facies metamorphism. The Paleozoic strata are mainly marine carbonate–clastic rocks. The Triassic marked a transition from marine to continental sedimentation, and the Cretaceous clastic rocks in the central mountainous area are folded with NW–SE-trending fold axes. The Cenozoic rocks occur mainly around and to the north of Hainan Island. The Paleogene strata consist of continental clastic rocks that overlie an angular unconformity developed on the underlying Cretaceous strata. The Neogene rocks record a change from continental to shallow-marine sedimentation. Unconsolidated Quaternary coastal sediments form the coastal terraces [5,22]. Hainan Island has also experienced significant magmatism, with Permian to Cretaceous granites being the most widely distributed igneous rocks. The volcanic rocks are primarily Cretaceous rhyolites, along with Neogene and Quaternary basalts [23].

 doi:10.20944/preprints202502.1758.v1

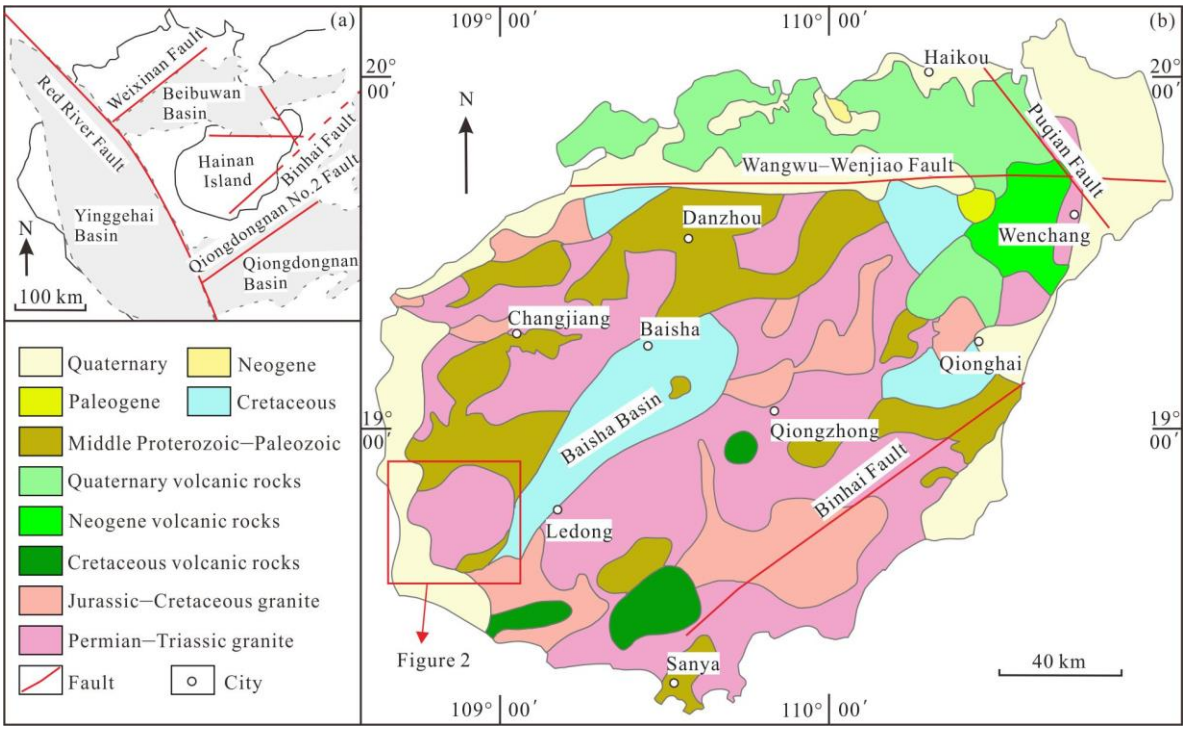

Figure 1. (a) Sketch map of basins around Hainan Island and (b) geological sketch map of Hainan Island (modified from [4]).

Jianfengling is located on southwestern Hainan Island and is a prominent landform in the western part of the national park, known as one of "China's Top Ten Most Beautiful Forest Parks". The main peak, with an altitude of 1412 m, contrasts sharply with the Yinggehai Basin and surrounding hilly terrain to the west. The Jianfeng pluton forms the geological core of the Jianfeng scenic area, and is located south of the Wangwu–Wenjiao Fault and at the southwestern margin of the Baisha graben basin. This nearly circular composite pluton (Figure 2) consists primarily of coarse-grained porphyritic biotite syenite granite of the Triassic Jianfengling unit, fine-grained porphyritic biotite syenite of the Heiling unit, and fine-grained biotite syenite of the Shouling unit, along with a small amount of quartz diorite of the late Permian Baishicun unit. The Jianfengling unit is the main lithology. The zircon U–Pb age of the middle section of the pluton is 249 ± 5 Ma [12], while the zircon U–Pb age of the pluton margin is 236 ± 2 Ma [10]. Therefore, the emplacement age of the Jianfeng pluton ranged between 249 and 236 Ma. Based on geochemical and isotopic analyses of the granite, it is an aluminous A-type granite that formed in a post-orogenic extensional setting [10].

 doi:10.20944/preprints202502.1758.v1

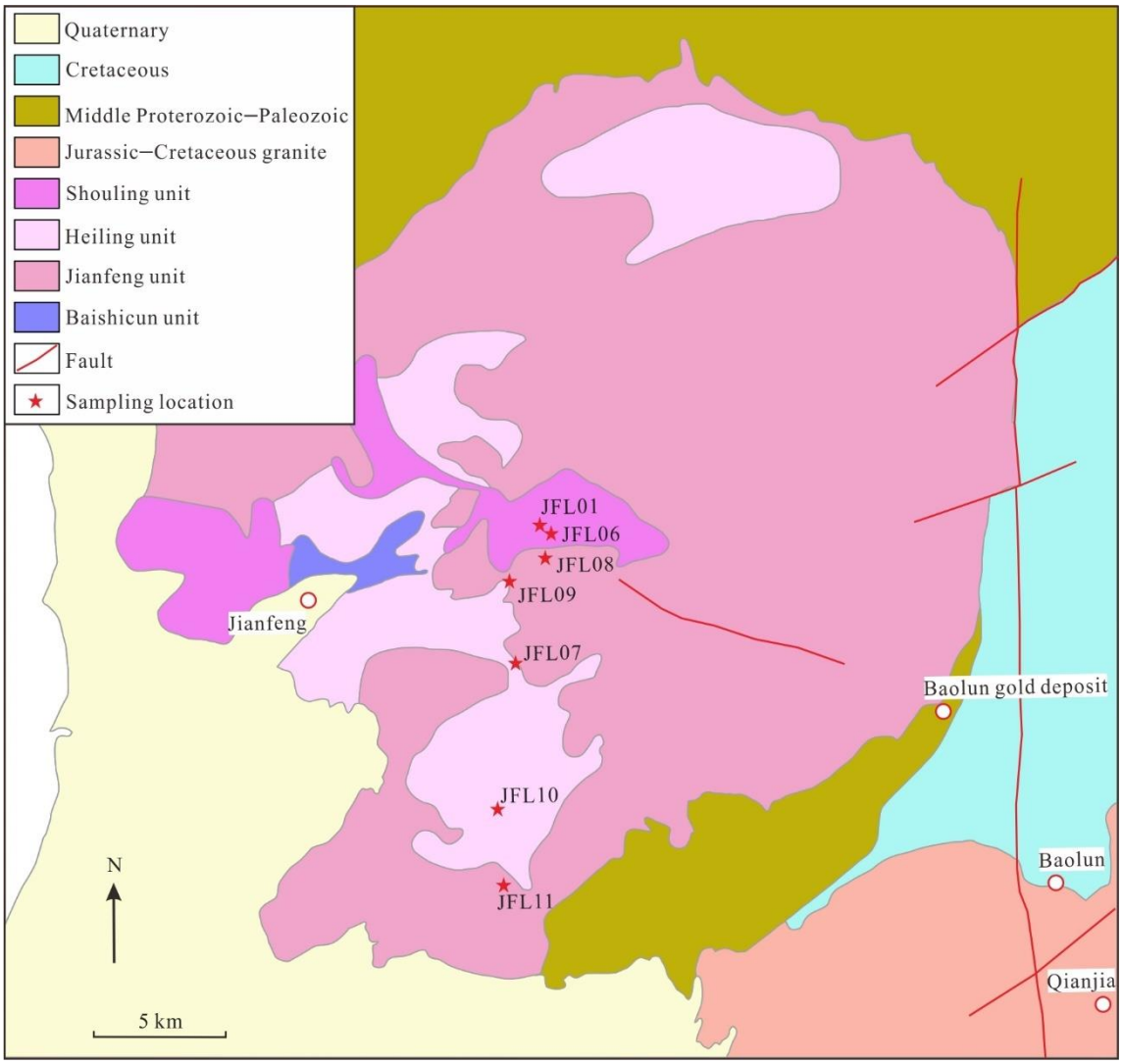

Figure 2. Geological sketch map of the Jianfeng area on Hainan Island (modified after [12]).

3. Methods

Seven samples of fresh granite were collected along a nearly straight transect from the top to the bottom of the Jianfeng mountain, over an altitude difference of ~200 m. Each sample weighed ~2.0 kg. Five samples were subjected to both ZFT and AFT analysis, and two samples were subjected to AFT dating. The samples were first coarsely crushed, finely crushed, and sieved, and then rinsed and subjected to density, magnetic, and heavy liquid separation to obtain apatite and zircon grains. The FT analyses were undertaken at the Low Temperature Thermochronology Laboratory of the School of Earth Sciences, China University of Geosciences, Wuhan, China. Zircon and apatite were mounted on Teflon sheets and in epoxy resin, respectively, and polished to expose grain centers, ensuring there were no scratches and smooth grain surfaces. The zircon and apatite were then etched separately. Zircon was etched in a 1:1 NaOH and KOH melt at a constant temperature of 228°C for 30–42 h, depending on factors such as the U content. Apatite was etched in 5.5 mol/L HNO_3 at a constant temperature of 21°C for 20 s. The experimental procedures followed the internationally accepted external detector method for FT analysis. The zircon and apatite were irradiated in a reactor using this external detector method. After irradiation, once the sample reached a safe radiation level, the mica sheet was etched in 48% HF at a constant temperature of 20°C for 18 min [24,25]. FT lengths were measured using an Axio Imager Z2m microscope (magnification 1000×) in conjunction with a fully automatic Autoscan FT system [26]. The ages were calculated using the Zeta correction method recommended by the International Union of Geological Sciences (IUGS), where the Zeta constant represents the weighted-mean of the standard samples [27]. The Zeta values obtained in this study were 331.4 ± 26.5 for apatite and 127.3 ± 6.8 for zircon.

 doi:10.20944/preprints202502.1758.v1

4. Results

4.1. ZFT Results

The ZFT results for the five samples of the Jianfeng granite are listed in Table 1. The pooled ZFT ages range from 63 ± 4 to 117 ± 8 Ma, and are younger than the crystallization age of the granite (249-236 Ma). This indicates the ages represent the cooling ages of the pluton after reaching the zircon annealing temperature. The χ^2 test values for the five samples are 71%–98%, much higher than the critical value of 5%. This suggests the single grain ages of each sample belong to the same age group and effectively record the thermal cooling history. In a FT age–elevation diagram (Figure 3), the ZFT ages display an inflection at 570 m and show a linear distribution from 73 Ma to 63 Ma, indicative of a rapid cooling event between 73 and 63 Ma. The exhumation rates before ~ 73 Ma and during 73 − 63 Ma are 0.02 km/Myr and 0.04 km/Myr, respectively.

Table 1. Fission-track dating results for zircon and apatite from the Jianfeng area, Hainan Island.

Sample	Elevation (m)	Analysis method	Number of grains	ρ_s (10^5/cm^2) (N_s)	ρ_i (10^5/cm^2) (N_i)	ρ_d (10^5/cm^2) (N_d)	P(χ^2) (%)	Central age (Ma)	Pooled age (Ma)	L (μm) (N)
JFL01	1404	AFT	22	6.2(388)	16.1(1002)	6.9(5045)	100	48.3 ± 5.8	43.9 ± 4.4	11.9 ± 1.0(14)
JFL06	1083	AFT	27	5.6(346)	15.1(937)	6.8(5043)	100	39.1 ± 4.8	41.7 ± 4.3	12.0 ± 1.1(14)
JFL08	871	AFT	41	3.1(637)	10.2(1575)	6.8(5039)	100	28.5 ± 4.3	33.7 ± 3.8	12.0 ± 1.2(24)
JFL09	707	AFT	23	6.5(406)	18.2(1133)	6.7(5037)	100	40.9 ± 5.3	39.8 ± 4.0	12.7 ± 1.5(14)
JFL07	570	AFT	28	5.7(356)	15.8(985)	6.8(5041)	100	38.7 ± 5.0	40.5 ± 4.1	12.6 ± 1.1(24)
JFL10	348	AFT	30	4.8(296)	17.5(1575)	6.7(5035)	100	29.3 ± 3.7	30.0 ± 3.0	12.7 ± 1.3(23)
JFL11	145	AFT	25	7.8(484)	44.2(2749)	6.6(5033)	100	18.1 ± 2.0	19.4 ± 1.8	12.3 ± 1.2(41)
JFL01	1404	ZFT	24	6.1(1742)	1.6(456)	4532(5221)	89	115 ± 11	108 ± 8	-
JFL06	1083	ZFT	23	6.3(1783)	1.9(554)	4520(5220)	92	88 ± 8	92 ± 7	-
JFL08	871	ZFT	22	3.8(1318)	0.9(318)	4494(5218)	98	120 ± 13	117 ± 8	-
JFL07	570	ZFT	25	5.9(1689)	2.7(762)	4507(5719)	90	64 ± 5	63 ± 4	-

 doi:10.20944/preprints202502.1758.v1

JFL11	145	ZFT	25	9.8(2786)	3.8(1078)	4482(5217)	71	72 ± 6	73 ± 5	-

Notes: ρ_s, ρ_i, and ρ_d are the spontaneous, induced, and standard track densities, respectively. N_s, N_i, and N_d are the spontaneous, induced, and standard track numbers, respectively. $P(\chi^2)$ is the χ^2 test value. N is the number of horizontally confined tracks. If $P(\chi^2) > 5$, Pooled age is used, otherwise Central age is used.

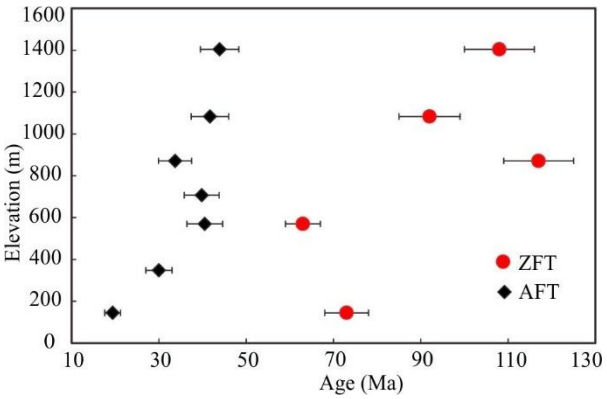

Figure 3. Fission-track age–elevation diagram for the Jianfeng area, Hainan Island.

4.2. AFT Results

The AFT results are presented in Table 1. The pooled AFT ages range from 19.4 ± 1.8 to 43.9 ± 4.4 Ma, and are much younger than the crystallization age of the Jianfeng granite. The χ2 test values for the seven samples are all 100%, greatly exceeding the critical value of 5% and indicating the ages are robust. This suggests that the single grain ages of each sample belong to the same age group. The average confined track length is relatively constant, but short (11.9–12.8 μm). The standard deviation ranges from 1.0 to 1.5 μm, which is slightly larger than expected, and the track length distribution is somewhat broad and positively skewed with a single peak (Figure 4). This is indicative of slow transport through the PAZ[25]. In a FT age–elevation diagram (Figure 3), the AFT ages show an inflection at 570 m and display a linear distribution from 44 Ma to 40 Ma, indicating a rapid cooling event between 44 and 40 Ma. The exhumation rates during 44 ~ 40 Ma and after ~ 40 Ma are 0.20 km / Myr and 0.02 km / Myr, respectively.

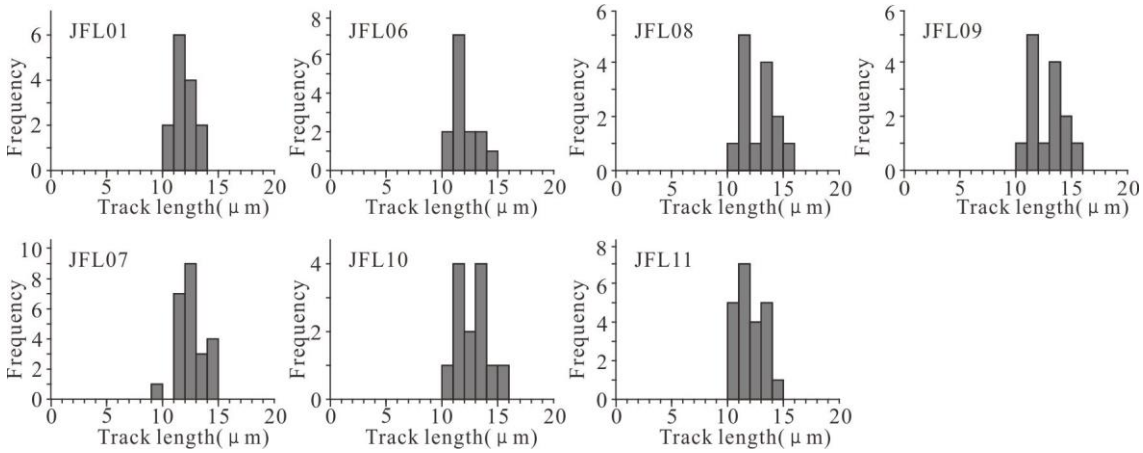

Figure 4. Histogram of apatite fission-track lengths for samples from the Jianfeng area on Hainan Island.

4.3. Modeling Results

We used the annealing model of Ketcham et al. [28] and a Monte Carlo approximation to simulate the thermal history of the samples. The initial conditions for the simulation are based on the AFT parameters, and the modeling was performed using HeFTy1.9.3 software. The initial simulation temperature was set to the ZFT annealing temperature of ~210°C [29]. The temperature range for the

 doi:10.20944/preprints202502.1758.v1

AFT PAZ is 60–110°C [30], while the final simulation temperature corresponds to the current surface temperature of 20°C. The model timeframe extends from 120 Ma in the Late Cretaceous to the present-day. Throughout the simulation, the model path was continuously refined in conjunction with the regional geological background and FT parameters to achieve the optimal results. The goodness-of-fit (GOF) value was used to assess the fit to the track length distributions and ages. A GOF value of >0.05 generally indicates an acceptable simulation result, while a value of >0.5 is considered a good simulation [31-33]. The results of the thermal modeling revealed that the five data models fit well, whereas the other data models (JFL09 and JFL11) are not discussed due to the GOF values being <0.5. Based on the thermal modeling, the geothermal gradient was estimated to be based on the thermal modeling 30°C/km [5,34], with a surface temperature of 20°C [5,34]. The cooling rate, and amount and rate of denudation in the different stages of the thermal history were estimated as follows.

The thermal histories of the five samples are similar (Figure 5), and generally exhibit a three-stage evolution. (1) During 73–40 Ma, the temperature decreased rapidly from the ZFT annealing temperature of 210°C to 76°C. The time difference is 33 Myr, and the temperature difference is 134°C, resulting in a cooling rate of 4.06 C/Myr, denudation of 4.47 km, and denudation rate of 0.14 km/Myr. (2) During 40–11 Ma, the temperature cooled gradually from 76°C to 56°C, near the top of the AFT PAZ. The time difference is 29 Myr and the temperature difference is 20°C, yielding a cooling rate of 0.69°C/Myr, denudation of 0.67 km, and denudation rate of 0.02 km/Myr. (3) From *ca*. 11 Ma to the present, the temperature cooled rapidly from 56°C to the current surface temperature of 20°C. The time difference is 11 Myr and the temperature difference is 36°C, yielding a cooling rate of 3.27 °C/Myr, denudation of 1.20 km, and denudation rate of 0.11 km/Myr. The total uplift and denudation of Jianfengling on Hainan Island since the Late Cretaceous (~73 Ma) is ~6.33 km.

 doi:10.20944/preprints202502.1758.v1

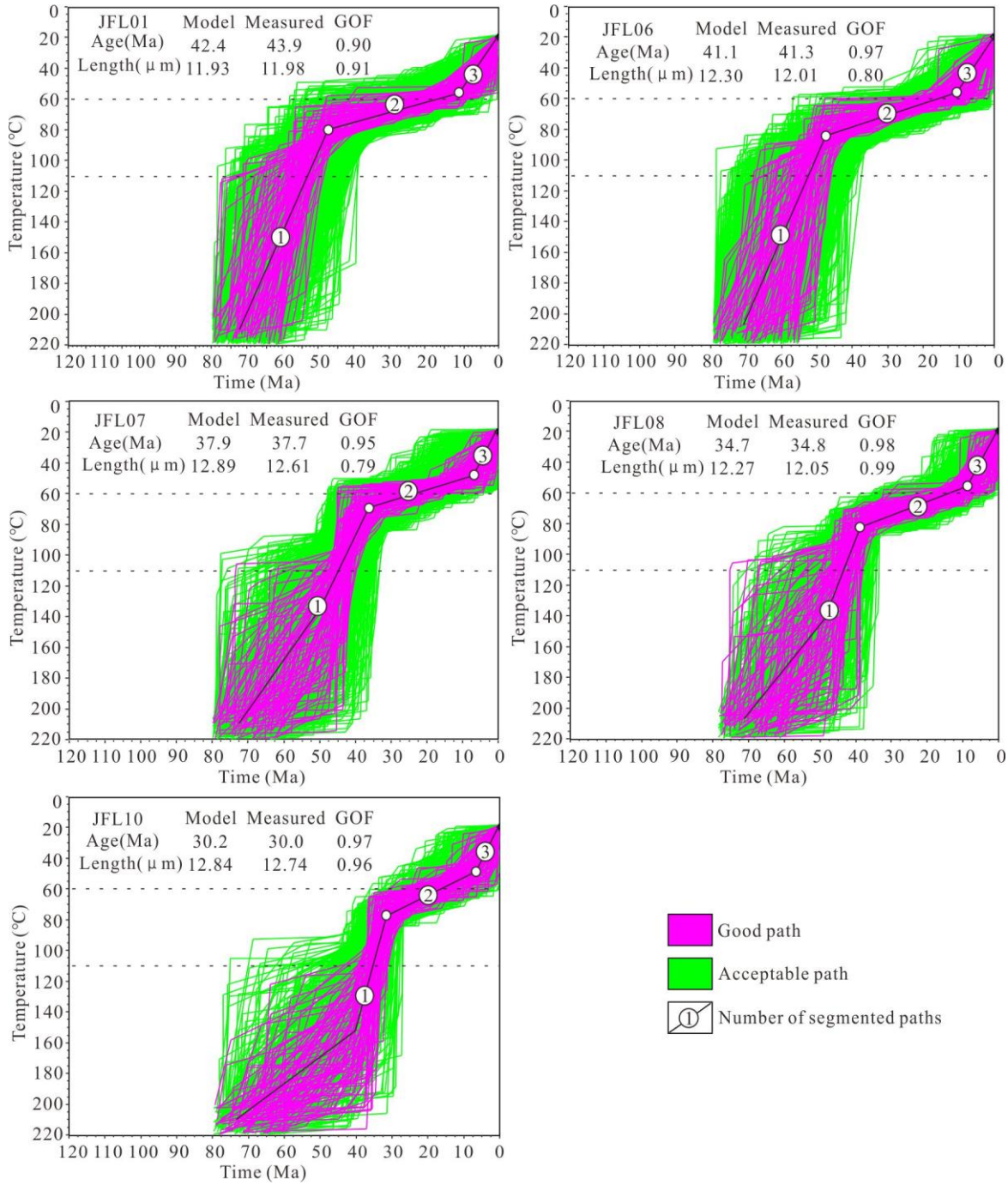

Figure 5. Simulation results of the thermal history of the Jianfeng area on Hainan Island.

 doi:10.20944/preprints202502.1758.v1

5. Discussion

In the Early Jurassic (205–180 Ma), Hainan Island transitioned from collision in the Tethyan tectonic domain to subduction in the Pacific tectonic domain [20,35]. During the Late Cretaceous, the subduction and retreat of the Paleo-Pacific Plate led to back-arc extension and the formation of the NE–SW-trending Baisha graben basin, A-type granites, and mafic dikes on Hainan Island [11]. Following this, northwestern Hainan Island was affected by collision of the Indian and Eurasian plates, eastern Hainan Island was affected by subduction of the Pacific Plate and Philippine Sea Plate, and south Hainan Island was influenced by subduction in the Proto-South China Sea and opening of the South China Sea [36,37].

5.1. Late Cretaceous to Middle Eocene Episodic Rapid Uplift and Denudation

From the Late Cretaceous to middle Eocene (73–40 Ma), the Jianfeng area on southwestern Hainan Island underwent episodic rapid uplift and denudation, characterized by a cooling rate of 4.06°C/Myr, denudation of 4.47 km, and denudation rate of 0.14 km/Myr. However, the FT age–elevation diagram (Figure 3) indicates that two rapid cooling events occurred at 73–63 and 44–40 Ma. This discrepancy can be attributed to the lack of FT length control on the simulation results over the temperature range of 210–110°C. Consequently, the rapid uplift and denudation in the Jianfeng area during this period can be described as episodic, with higher rates during 73–63 and 44–40 Ma.

At the end of the Late Cretaceous (73–63 Ma), southeastern China was affected by mid-ocean ridge spreading in the Proto-South China Sea and subduction of the Pacific Plate, which replaced the Paleo-Pacific Plate [38]. The Neo-Tethys Ocean had not yet closed and the Indian Plate had not yet begun to collide with the Eurasian Plate [2,39]. During this period, rapid uplift and denudation of southeastern Hainan Island began earlier (82–63 Ma) than on southwestern Hainan Island (73–63 Ma) [40]. This suggests that the driving mechanisms of the rapid uplift and denudation of Hainan Island originated from its southeastern region (Figure 6a1). Field data indicate that the Cretaceous strata in the Baisha Basin in the central mountainous area of Hainan Island experienced NW–SE compression, resulting in the formation of oblique folds and an angular unconformity with the overlying strata. Similarly, the Late Cretaceous granitic intrusions on the island record NW–SE compression on conjugate joints, but there is no record of magmatism at the end of the Late Cretaceous (*ca*. 80 Ma) [11]. Therefore, the mechanisms of rapid uplift and denudation of Hainan Island at the end of the Late Cretaceous were likely mid-ocean ridge push from the Proto-South China Sea. Some studies have also proposed that a subduction and compression event related to the Pacific Plate occurred in southeastern China at the end-Cretaceous, based on the development of large-scale NE–SW-trending thrust faults in South China [41]. The NW–SE compressive stress caused by the subduction of the Pacific Plate is thought to have gradually weakened from north to south along the continental margin of South China. However, the onset of rapid cooling and denudation on Hainan Island, located on the southern margin of South China (*ca*. 82 Ma), is consistent with the onset of compression recorded along the continental margin of South China (*ca*. 80 Ma) [6,7]. Consequently, the rapid uplift and denudation of Hainan Island at the end of the Late Cretaceous could not have been due to subduction of the Pacific Plate.

 doi:10.20944/preprints202502.1758.v1

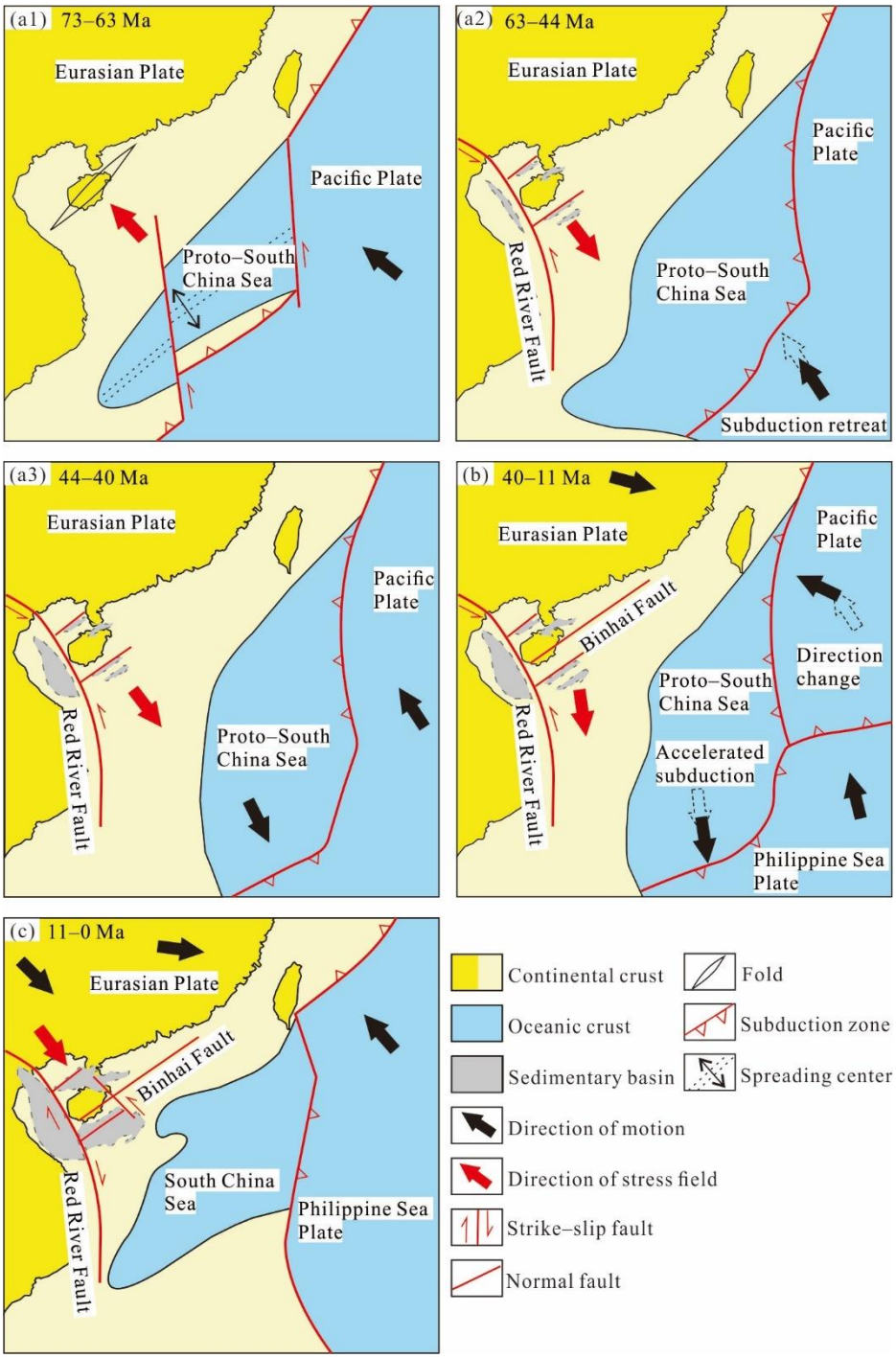

Figure 6. Mesozoic–Cenozoic tectonic evolution of Hainan Island (modified after [40]). (a1) At the end of the Late Cretaceous (73–63 Ma), mid-ocean ridge spreading in the Proto-South China Sea generated NW–SE-oriented compressional stress. (a2) During the early Paleocene to middle Eocene (63–44 Ma), the Pacific Plate subducted and retreated, causing the local stress field to change to NW–SE extension, which initiated basin extension and rifting around Hainan Island. (a3) From the middle Eocene to late Oligocene (44–40 Ma), abrupt extension and subsidence of the Yinggehai Basin increased the height difference between the Jianfengling area and the Yinggehai Basin, leading to rapid denudation. (b) From the middle Eocene to middle Miocene (40–11 Ma), large amounts of sediment transported by the Red River from the southeastern Qinghai–Tibetan Plateau quickly infilled the Yinggehai Basin, eliminating the elevation difference between the Jianfengling area and the adjacent Yinggehai Basin. (c) From the middle Miocene to present (11–0 Ma), the remote effects of the collision between the India and Eurasia plates produced NW–SE-oriented compression.

In the Cenozoic (*ca*. 63 Ma), the Pacific Plate subducted and retreated, causing a change in the local stress field to NW–SE extension [42]. As a result, the basins around Hainan Island began to

 doi:10.20944/preprints202502.1758.v1

undergo extension, rifting, and sediment deposition (Figure 6a2). In the middle Eocene (44-40 Ma), the Pacific Plate along the eastern margin of Eurasia continued to subduct, while the Indian Plate collided with the Eurasian Plate along its western margin [43,44]. At this time, oceanic lithosphere of the Proto-South China Sea on the southeastern margin of Eurasian Plate was subducting southward beneath the Borneo Block [40]. The Pacific Plate and Hainan Island were separated by the subduction zone in the Proto-South China Sea. The compressive stress generated by subduction was poorly transmitted to Hainan Island. The southeastern part of Hainan Island underwent slow denudation during this period [40], and thus the driving force of the rapid uplift and denudation during the middle Eocene (44–40 Ma) could not have been due to subduction in the Proto-South China Sea. The intense collision between the Indian and Eurasian plates caused the asthenospheric mantle beneath the Eurasian Plate to escape in a northeast direction. Previous studies have documented a trend of progressively later uplift and denudation, as well as tectonic inversion, from the continental margin to oceanic basin in eastern South China. This is interpreted to record the remote effects of collision between the Indian and Eurasian plates during the middle Eocene, resulting in the transmission of compressive stress from west to east [45]. However, no inversion structures have been found in the basins around Hainan Island that formed during this period and, in fact, rifting continued [4]. The relatively rapid denudation on the island could not have resulted from the remote compressive stress caused by the collision of the Indian and Eurasian plates. Another significant result of the collision on the western margin of Eurasian Plate was the large-scale, left-lateral, strike-slip activity of the Red River Fault Zone, which led to the sudden expansion and subsidence of the Yinggehai pull-apart basin (Figure 6a3). This significantly increased the height difference between the peak area on southwestern Hainan Island and the Yinggehai Basin, resulting in rapid denudation during this period.

5.2. Middle Eocene to Middle Miocene Slow Denudation

From the middle Eocene to middle Miocene (40–11 Ma), the Jianfeng area on southwestern Hainan Island underwent slow denudation, with a cooling rate of 0.69 °C/Myr, denudation of 0.67 km, and denudation rate of 0.02 km/Myr. During this period, the compressive stress generated by subduction of the Pacific Plate to the east could not be transmitted to Hainan Island (Figure 6b). The Indian and Eurasian plates to the west continued to experience a hard continental collision [43], and subduction in the Proto-South China Sea to the south decreased [46]. Previous studies indicate that the Proto-South China Sea underwent accelerated subduction at 40–24 Ma, and FT data for southeastern Hainan Island record a brief period of rapid uplift [22,40,47]. However, the Jianfengling area continued to undergo slow denudation during 40–11 Ma, suggesting that accelerated subduction in the Proto-South China Sea primarily affected denudation on eastern Hainan Island. Some studies have also proposed that rapid denudation occurred on southern Hainan Island during the Oligocene [5]. However, the average confined AFT length from this study is relatively uniform, but short (11.9–12.8 μm), with a large standard deviation (1.0–1.5 μm), indicating a rapid cooling event did not occur on Hainan Island during the Oligocene. This is supported by the AFT length data and the geodynamics of the Cenozoic extensional graben basins surrounding Hainan Island.

The Beibuwan, Yinggehai, and Qiongdongnan basins around Hainan Island are the primary accumulation sites for denuded materials from the northern margin of the South China Sea. The source areas of these materials include the southeastern Qinghai–Tibetan Plateau, eastern Vietnam, and Hainan Island, with the Qinghai–Tibetan Plateau being the main source. The sediments are primarily transported by the Red River, making the southeastern region a significant contributor [48]. Although the Indian and Eurasian plates continue to collide, the rotation of the Indosinian Block and left-lateral slip on the Red River Fault have caused further extension in the Yinggehai sub-basin on southwestern Hainan Island. During the middle uplift stage of the Qinghai–Tibetan Plateau (40–25 Ma), the thickness and altitude of the crust increased significantly [49]. This uplift led to a substantial influx of sediment from the southeastern Qinghai–Tibetan Plateau, which quickly filled the Yinggehai Basin. Consequently, this eliminated the elevation difference between the Jianfengling area and the adjacent Yinggehai Basin.

 doi:10.20944/preprints202502.1758.v1

5.3. Middle Miocene to Present Rapid Cooling and Denudation

From the middle Miocene to the present (11–0 Ma), the Jianfeng area has experienced strong cooling and erosion, with a cooling rate of 3.27 C/Myr, denudation of 1.20 km, and denudation rate of 0.11 km/Myr. This is consistent with the increased sedimentation recorded in the surrounding basins since the middle Miocene [50]. During the middle Miocene (*ca*. 11 Ma), subduction in the Proto-South China Sea south of Hainan Island was accompanied by a cessation of the expansion of the South China Sea, while the Philippine Sea Plate to the east was wedged in a north-northwest direction [42]. In the Qiongdongnan Basin on the island and around its periphery, a series of NW–SE-trending left-lateral strike-slip faults, as represented by the Puqian Fault, developed, cutting the older NE–SW-trending coastal faults (Figure 6c). However, there are no inversion structures in the Qiongdongnan Basin to the east of Hainan Island. This indicates the strong compressive stress generated by wedging of the Philippine Sea Plate to the east absorbed deformation by strike-slip movement, with minimal vertical movement. Paleomagnetic data further support this, showing that Hainan Island has rotated counterclockwise by ~9° relative to the Philippine Sea Plate [51]. In contrast, the Beibuwan Basin to the north of Hainan Island contains NE–SW-trending inverted folds, with the intensity of inversion decreasing from northwest to southeast. Similarly, the Yinggehai Basin on southwestern Hainan Island contains inverted folds [50], indicating that Hainan Island was subjected to NW–SE compressive stress resulting from the collision between the Indian and Eurasian plates. Since the middle Miocene, the Red River–Ailaoshan Fault Zone on the southeastern margin of the Qinghai–Tibetan Plateau has been reactivated, leading to a marked increase in the component of vertical movement [17,52]. This has triggered NW–SE compressive stress along the northern margin of the South China Sea, including Hainan Island. Since *ca*. 5 Ma, although FT thermal modeling indicates that all samples were located in the upper AFT PAZ, increased rainfall associated with strengthening of the Southeast Asian monsoon has accelerated the denudation rate [53].

6. Conclusions

From the Late Cretaceous to middle Eocene (73–40 Ma), the Jianfeng area experienced episodic rapid uplift and denudation. During this period, the cooling rate and the amount and rate of denudation were 4.06°C/Myr, 4.47 km, and 0.14 km/Myr, respectively. At the end of the Late Cretaceous (73–63 Ma), these changes were initiated by the mid-ocean ridge spreading in the Proto-South China Sea. During the middle Eocene (44–40 Ma), significant left-lateral strike-slip movement along the Red River Fault caused the Yinggehai pull-apart basin to abruptly expand and subside, resulting in a notable increase in the elevation difference between the Jianfengling area and Yinggehai Basin.

From the middle Eocene to middle Miocene (40–11 Ma), the Jianfeng area experienced slower denudation. During this period, the cooling rate, and amount and rate of denudation were 0.69°C/Myr, 0.67 km, and 0.02 km/Myr, respectively. A large volume of sediment sourced from the southeastern Qinghai–Tibetan Plateau was transported by the Red River, which rapidly filled the Yinggehai Basin. This influx of sediment eliminated the elevation difference between the Jianfeng area and the adjacent Yinggehai Basin.

From the middle Miocene to present (11–0 Ma), the Jianfeng area has again undergone rapid cooling and erosion. During this period, the cooling rate, and amount and rate of denudation were 3.27°C/Myr, 1.20 km, and 0.11 km/Myr, respectively. The remote effects of the collision between the Indian and Eurasian plates subjected Hainan Island to significant compression, resulting in this rapid uplift and denudation.

Author Contributions: D.L.: Conceptualization, Methodology, Writing—review & editing. G.X.: Methodology, Formal analysis, Writing—original draft. Y.Z.: Supervision, Investigation, Methodology, Writing—review & editing. Z.G.: Methodology, Writing—review & editing. Z.H.: Writing—review & editing. C.W.: Writing—review & editing. Z.Z.: Writing—review & editing. Q.Y.: Writing—review & editing. All authors have read and agreed to the published version of the manuscript.

Funding: This research was funded by the Hainan Provincial Natural Science Foundation of China (421RC1109), the Basic Fund from the Key Laboratory of Deep-Earth Dynamics of Ministry of Natural Resources

 doi:10.20944/preprints202502.1758.v1

(JKYQN202314), and the Open Research Fund of Hainan Key Laboratory of Marine Geological Resources and Environment (HNHYDZZYHJKF014).

Data Availability Statement: Not applicable.

Acknowledgments: During the field investigation and sample collection process, the Hainan Jianfeng Forestry Bureau provided invaluable assistance, and we would like to express our sincere gratitude.

Conflicts of Interest: The authors declare no conflicts of interest.

References

1. 1. Metcalfe Ian. Gondwana dispersion and Asian accretion: Tectonic and palaeogeographic evolution of eastern Tethys. Journal of Asian Earth Sciences, 2013, 66: 1-33.
2. 2. Hall Robert. Late Jurassic–Cenozoic reconstructions of the Indonesian region and the Indian Ocean. Tectonophysics, 2012, 570: 1-41.
3. 3. Lei Chao, Ren Jianye, Pang Xiong. Rift structures and its related unconformities on and adjacent the Dongsha Rise: insights into the nature of the high-velocity layer in the northern South China Sea. Marine Geophysical Research, 2019, 40: 99-110.
4. 4. Wu Shiguo, Lu Xiangyang, Li Gang, Genyuan Long. Tectonics and discrepant evolution of Cenozoicsedimentary basins adjacent Hainan Island. Acta Geologica Sinica, 2024, 98(1): 16-30(in Chinese with English abstract).
5. 5. Shi Xiaobin, Kohn Barry, Spencer Steven, Guo Xingwei, Li Yamin, Yang Xiaoqiu, Shi Hongcai, Gleadow Andrew. Cenozoic denudation history of southern Hainan Island, South China Sea: constraints from low temperature thermochronology. Tectonophysics, 2011, 504(1-4): 100-115.
6. 6. Shi Xiaobin, Kohn Barry, Yu Chuanhai, Tian Yuntao, Li Guangwei, Zhao Peng. Thermo-tectonic history of coastal NW South China Sea: A low-temperature thermochronology study. Tectonophysics, 2022, 833: 229-344.
7. 7. Yan Yi, Carter Andrew, Palk Carl, Brichau Stéphanie, Hu Xiaoqiong. Understanding sedimentation in the Song Hong–Yinggehai Basin, South China Sea. Geochemistry, Geophysics, Geosystems, 2011, 12(6): 1-15.
8. 8. Zhou Jianping, Li Sanzhong, Liu Yongjiang, Liu Boran, Li Weimin, Wang Guangzeng, Jiang Liwei, Zhou Tong, Li Zunting, Feng Zhiqiang. Differential Uplift Triggered Basin-And-Range System: Evidence From Low-Temperature Thermochronology in Eastern NE Asia. Tectonics, 2024, 43(1): 1-25.
9. 9. Wang Xiuxi, Zattin Massimiliano, Yang Yu, Tao Jia, Liu Huiming, Zhang Yanbo, Wang Hong, Pang Bozhong, Wang Linbing, Ji Minxiao. Multiple Exhumation Stages During the Cenozoic Evolution of the Northeast Tibetan Plateau. Tectonics, 2024, 43(3): e2023TC007850.
10. 10. Lin Di, Wan Sheng, Hu Zailong, Lyu Changyan, Shan Qiang, Liang Xiao, Wei Changxin, Yuan Qinmin, Peng Gao. Geochemical characteristics of bimodal intrusive complex in Baolun gold deposit, Hainan island and its implications for regional gold mineralization. Mineral Deposits, 2023, 42(06): 1229-1246(in Chinese with English abstract).
11. 11. Cai Jianxin, Wu Chuanjun, Xu Deru, Hou Maozhou, Shan Qiang, Zhu Yuhua, Lin Di. Structural analysis of the Baolun gold deposit, Hainan Island, South China: Implications for metallogeny. Ore Geology Reviews, 2017: 253-269.
12. 12. Xie Caifu, Zhu Jinchu, Ding Shijiang, Zhang Yeming, Chen Mulong, Fu Yangrong, Fu Taian, Zhihong Li. Age and petrogenesis of the Jianfengling granite and its relationship to metallogenesis of the Baolun gold deposit, Hainan Island. Acta Petrologica Sinica, 2006(10): 2493-2508(in Chinese with English abstract).
13. 13. Gallagher Kerry, Brown Roderick, Johnson Christopher. Fission track analysis and its applications to geological problems. Annual Review of Earth and Planetary Sciences, 1998, 26(1): 519-572.
14. 14. Reiners P. W., Brandon M. T. Using thermochronology to understand orogenic erosion. Annual Review of Earth and Planetary Sciences, 2006, 34: 419-466.
15. 15. Gao Peng, Hu Jie, Hu Shengbiao. Mesozoic and Cenozoic Tectono-Thermal Reconstruction of the Southern Ordos Basin: Revealed by Apatite Fission Track and (U-Th)/He Dating. Minerals, 2024, 14(2).

 doi:10.20944/preprints202502.1758.v1

16. 16. Li Shiyu, Yuan Wanming, Zhao Zhidan, Zhang Aikui, Dong Guochen, Li Xiaowei, Sun Wenli. Process and Mechanism of Exhumation in the Southern Altai Mountains, Northwest China. Minerals, 2024, 14(12).
17. 17. Wang Ying. Features of Hainan Island coastal environment. Marine Geology Letters, 2002, 18(3): 1-9.
18. 18. Liu Yang., Fang Nianqiao., Wang Zhongbo. The geochemical characteristics of Cretaceous volcanics in southern Hainan Island and implications for tectonic evolution in the South China Sea. Frontiers in Earth Science, 2023, 11.
19. 19. Zhang Limin, Cui Xiang, Yang Yong, Chen Si, Zhao Bin, Deng Xiguang. Precambrian Tectonic Affinity of Hainan and Its Evolution from Columbia to Rodinia. Minerals, 2023, 13(10).
20. 20. He Huiying, Wang Yuejun, Cawood Peter A, Qian Xin, Zhang Yuzhi, Zhao Guofeng. Permo-Triassic granitoids, Hainan Island, link to Paleotethyan not Paleopacific tectonics. Geological Society of America Bulletin, 2020, 132(9-10): 2067-2083.
21. 21. Yan Quanshu., Shi Xuefa., Castillo Paterno R. The late Mesozoic-Cenozoic tectonic evolution of the South China Sea: A petrologic perspective. Journal of Asian Earth Sciences, 2014, 85: 178-201.
22. 22. Cullen Andrew, Reemst Paul, Henstra Gijs, Gozzard Simon, Ray Anandaroop. Rifting of the South China Sea: new perspectives. Petroleum Geoscience, 2010, 16(3): 273-282.
23. 23. Jiang Xiaoyan, Dilek Yildirim, Li Xianhua. Cretaceous magmatic arc in Hainan and the peri-South China Sea as evidenced by geochemical fingerprinting of granitoids in the region. Geoscience Frontiers, 2024, 15(5).
24. 24. Bellemans F, De F, Van Den P. Composition of SRM and CN U-doped glasses: Significance for their use as thermal neutron fluence monitors in fission track dating. Radiation measurements, 1995, 24(2): 153-160.
25. 25. Yuan Wanming, Dong Jinquan, Shicheng Wang, Carter Andrew. Apatite fission track evidence for Neogene uplift in the eastern Kunlun Mountains, northern Qinghai–Tibet Plateau, China. Journal of Asian Earth Sciences, 2006, 27(6): 847-856.
26. 26. Cao Kai, Replumaz Anne, Tian Yuntao, Husson Laurent, Wang Guocan , Shen Tianyi, Reiners Peter, Bernet Matthias, Beek Peter Van Der. Southwestward growth of plateau surfaces in eastern Tibet. Earth-Science Reviews, 2022, 232.
27. 27. Hurford Anthony J. Standardization of fission track dating calibration: Recommendation by the Fission Track Working Group of the IUGS Subcommission on Geochronology. Chemical Geology: Isotope Geoscience Section, 1990, 80(2): 171-178.
28. 28. Ketcham Richard A, Carter Andrew, Donelick Raymond A, Barbarand Jocelyn, Hurford Anthony J. Improved modeling of fission-track annealing in apatite. American Mineralogist, 2007, 92(5-6): 799-810.
29. 29. Bernet Matthias. A field-based estimate of the zircon fission-track closure temperature. Chemical Geology, 2009, 259(3-4): 181-189.
30. 30. Wagner Günther A. Cooling ages derived by apatite fission-track, mica Rb-Sr and K-Ar dating; the uplift and cooling history of the Central Alps. Mem. Inst. Geol. Mineral., Univ. of Padova, 1977, 30: 1-27.
31. 31. Ye Zhanghuang, Yin Bin, Liu Jiaqi, Wang Anjian, Yan Qiang. Uplift and denudation of Mt Sanqingshan Geopark, Jiangxi Province, China. International Geology Review, 2014, 56(15): 1873-1883.
32. 32. Sobel Edward R, Strecker Manfred R. Uplift, exhumation and precipitation: tectonic and climatic control of Late Cenozoic landscape evolution in the northern Sierras Pampeanas, Argentina. Basin Research, 2003, 15(4): 431-451.
33. 33. Yuan Wan Ming, Yang Zhi Qiang, Zhang Zhao Chong, Deng Jun. The uplifting and denudation of main Huangshan Mountains, Anhui Province, China. Scientia Sinica(Terrae), 2011, 54(8): 1168-1176.
34. 34. Shi Junhua, Han Shuai, Du Jianjun, Han Jianen, Sun Dongxia, Daogong Hu. Surface process responses to the expansion of the northern South China Sea:Age evidence of apatite fission tracks from Wuzhi Mountains, Hainan Island. Acta Geologica Sinica, 2024, 98(2): 421-432(in Chinese with English abstract).
35. 35. Zhou Xinmin, Sun Tao, Shen Weizhou, Shu Liangshu, Niu Yaoling. Petrogenesis of Mesozoic granitoids and volcanic rocks in South China: a response to tectonic evolution. Episodes Journal of International Geoscience, 2006, 29(1): 26-33.
36. 36. Ren Jianye, Tamaki Kensaku, Li Sitian, Junxia Zhang. Late Mesozoic and Cenozoic rifting and its dynamic setting in Eastern China and adjacent areas. Tectonophysics, 2002, 344(3-4): 175-205.

37. 37. Jianye Ren. Genetic dynamics of China offshore cenozoic basins. Earth Science, 2018, 43(10): 3337-3361(in Chinese with English abstract).
38. 38. Suo Yanhui, Li Sanzhong, Jin Chong, Zhang Yong, Zhou Jie, Li Xiyao, Wang Pengcheng, Liu Ze, Wang Xinyu, Somerville Ian. Eastward tectonic migration and transition of the Jurassic-Cretaceous Andean-type continental margin along Southeast China. Earth-Science Reviews, 2019, 196: 102884.
39. 39. Xu Zhiqin, Yang Jingsui, Li Haibing, Ji Shaocheng, Zhang Zemin, Yan Liu. On the Tectonics of the India-Asia Collision. Acta Geologica Sinica, 2011, 85(01): 1-33(in Chinese with English abstract).
40. 40. Lin Di, Zheng Yong, Hu Zailong, Liang Xiao, Wei Changxin, Qinmin Yuan. Tectonic activity history and its dynamic mechanism of the Binhai fault, Hainan Island: New evidences from apatite and zircon fission track analyses. Acta Geologica Sinica, 2024, 98: 1-13(in Chinese with English abstract).
41. 41. Xing Guangfu, Chen Rong, Yang Zhuliang, Zhou Yuzhang, Li Longming, Jiang Yang, Zhihong Chen. Characteristics and tectonic setting of Late Cretaceous volcanic magmatism in the coastal Southeast China. Acta Petrologica Sinica, 2009, 25(1): 77-91(in Chinese with English abstract).
42. 42. Wu Jonny, Suppe John, Lu Renqi, Kanda Ravi. Philippine Sea and East Asian plate tectonics since 52 Ma constrained by new subducted slab reconstruction methods. Journal of Geophysical Research: Solid Earth, 2016, 121(6): 4670-4741.
43. 43. P Tapponnier, R Lacassin, Ph H Leloup, U Schärer, Zhong Dalai, Wu Haiwei, Liu Xiaohan, Ji Shaocheng, Zhang Lianshang, Zhong Jiayou. The Ailao Shan/Red River metamorphic belt: tertiary left-lateral shear between Indochina and South China. Nature, 1990, 343(6257): 431-437.
44. 44. Patriat Philippe, Achache Jose. India–Eurasia collision chronology has implications for crustal shortening and driving mechanism of plates. Nature, 1984, 311(5987): 615-621.
45. 45. Wang Xinyu, Suo Yanhui, Li Sanzhong, Cao Xianzhi, Li Xiyao, Zhou Jie, Wang Pengcheng, Chong Jin. Cenozoic uplift history and its dynamic mechanism along the eastern continental margin of South China. Acta Petrologica Sinica, 2020, 36(6): 1803-1820(in Chinese with English abstract).
46. 46. Hall Robert. Australia–SE Asia collision: plate tectonics and crustal flow. Geological Society London Special Publications, 2011, 355(1): 75-109.
47. 47. Taylor Brian, Hayes Dennis E. Origin and history of the South China Sea basin. Geophysical Monograph Series, 1983, 27: 23-56.
48. 48. Clift Peter D, Sun Zhen. The sedimentary and tectonic evolution of the Yinggehai–Song Hong basin and the southern Hainan margin, South China Sea: Implications for Tibetan uplift and monsoon intensification. Journal of Geophysical Research: Solid Earth, 2006, 111(B6).
49. 49. Li Deyong, Jiang Xiaodian, Gong Wei, Li Chaoyang. Tectonic uplift along the northeastern margin of the Qinghai-Tibetan Plateau: Constraints from the lithofacies sequence and deposition rate of the Qaidam Basin. Tectonophysics, 2022, 827: 229279.
50. 50. Li Sanzhong, Suo Yanhui, Liu Xin, Dai Liming, Yu Shan, Zhao Shujuan, Ma Yun, Wang Xiaofei, Cheng Shixiu, An Huiting, Xue Youchen, Xiong Lijuan, Cao Xianzhi, Liqing Xu. Basin dynamics and basin groups of the South China Sea. Marine Geology & Quaternary Geology, 2012, 32(6): 55-78(in Chinese with English abstract).
51. 51. Fu Lulu, Shen Zhongyue, He Li, Dong Chuanwan, Cheng Xiaogan, Tang Limei, Shufeng Yang. Cretaceous Paleomagnetic Results from Hainan Island and Its Tectonic Implications. Acta Geologica Sinica, 2010, 84(2): 183-194(in Chinese with English abstract).
52. 52. Zheng Yong, Pan Jiawei, Li Haibing, Wang Yang, Gong Zheng, Bai Mingkun. Formation of the Great Bend and Enhanced Quaternary Incision of the Upper Yangtze River: New Insights from Low-Temperature Thermochronology and Tributary Morphology. Lithosphere, 2024, 2023(14): 1-18.
53. 53. Clift Peter D, Wan Shiming, Blusztajn Jerzy. Reconstructing chemical weathering, physical erosion and monsoon intensity since 25 Ma in the northern South China Sea: a review of competing proxies. Earth-Science Reviews, 2014, 130: 86-102.

 doi:10.20944/preprints202502.1758.v1

disclaim responsibility for any injury to people or property resulting from any ideas, methods, instructions or products referred to in the content.